Research Article Vol. 7, No. 1 / January 2020 / Optica 7

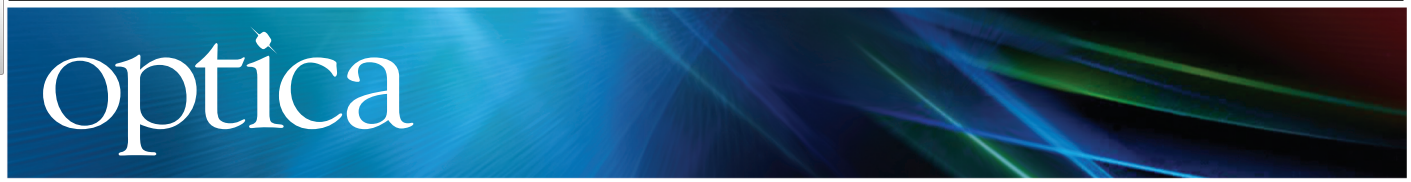

Reconfigurable nonlinear nonreciprocal transmission in a silicon photonic integrated circuit

Ang Li[1,2,3,*] and Wim Bogaerts[1,2]

[1]Photonics Research Group, Ghent University-IMEC, Department of Information Technology, Ghent University, 9052 Gent, Belgium
[2]Center for Nano- and Biophotonics, Ghent University, 9052 Gent, Belgium
[3]Current address: Department of Electrical and Computer Engineering, University of California, 9500 Gilman Drive, La Jolla, San Diego, California 92093, USA
*Corresponding author: angli@ucsd.edu

Received 2 August 2019; revised 14 November 2019; accepted 22 November 2019 (Doc. ID 374522); published 2 January 2020

We present a programmable silicon photonic integrated circuit (PIC) that can be configured to show nonlinear nonreciprocal transmission at high optical input power. Nonreciprocal transmission in PICs is of fundamental importance in various fields. Despite diverse approaches to generate nonreciprocal transmission, the research on efficient control of this effect is still scarce. The silicon PIC presented here has programmable linear and nonlinear behavior using integrated phase shifters. In the nonlinear regime (high optical power), the device can be configured to be either reciprocal or nonreciprocal between opposite propagation directions with over 30 dB extinction ratio and only 1.5 dB insertion loss. More importantly, the high/low transmission direction can be dynamically reconfigured. Furthermore, nonreciprocal transmission based on nonlinearities usually requires the optical field in both propagation directions to be high, in order to induce a large extinction ratio. For our circuit, only the forward-propagating light needs to have high power to enjoy low-loss transmission while the backward propagating light will always suffer a high rejection. Besides this nonreciprocal behavior, the circuit also offers the ability for all-optical functions, such as switching, optical compute gates, or optical flip-flops, thanks to its unique controllable nonlinear behavior. This work can trigger new research efforts in nonreciprocal photonics circuits.

https://doi.org/10.1364/OPTICA.7.000007

1. INTRODUCTION

Nonreciprocal behavior in photonic integrated circuits (PIC) is of fundamental interest and importance for signal processing, optical computing, and all-optical logic [1,2]. Nonreciprocal behavior is also the key phenomenon behind optical isolators. However, the constraints of the Lorentz reciprocity theorem make it impossible to generate such a behavior in a linear, nonmagnetic, and time-independent medium, which is the case for most PIC platforms. Accordingly, efforts to generate nonreciprocal transmission in PICs rely upon breaking the time-invariance of the medium, using magneto-optic materials that show direction-dependent permittivity tensors and introducing nonlinearity into the system. The first approach proves to be a promising engineering solution towards complete on-chip isolation, but it typically requires electro-optical modulation using complicated accompanying electronics and introduces significant power consumption. Moreover, it can induce unwanted frequency mixing due to the sidebands caused by the modulation [3–6]. Magneto-optic materials (e.g., as a waveguide cladding) in integrated optical structures (typically ring resonators) have also been demonstrated for nonreciprocal transmission and optical isolators [7–12]. However, the path towards usable nonreciprocal devices is nontrivial due to the engineering difficulties of integrating those magneto-optic materials into established PIC platforms. The third approach is to introduce asymmetric nonlinear effects like Brillouin-induced transparency, optomechanically induced transparency, nonreciprocal Kerr effect in a silica, thermal nonlinearities in asymmetric ring resonators, or PT symmetric devices [5,13–21]. Because these devices rely on nonlinear optical effects, their nonreciprocal behavior depends on the optical intensity. Therefore, they cannot really function as an optical isolator [2], but the nonlinear nonreciprocal transmission can be used for switching and all-optical signal processing. Despite several successful experimental demonstrations of such nonlinear nonreciprocal behavior, efficient control of the transmission characteristics remains challenging.

In this paper, we report a novel generation of controllable nonlinear nonreciprocal transmission in a mixed cavity system triggered by thermally induced nonlinearities at high optical input intensity, and the structure could also be implemented in other PIC platforms with other intensity-induced nonlinearities such as the Kerr effect [22]. Similar to the methods based on optomechanically induced transparency and Bruillouin-induced transparency

[13–15,17], our method also involves a type of induced transparency, which is the optical analogue of electromagnetically induced transparency (EIT), a phenomenon originating in atom physics [23]. Demonstrating EIT in (integrated) optics has already attracted significant interest, as it is one of the most promising techniques to implement slow light structures for optical buffers or storage [24–27]. Our circuit further takes advantage of this to realize a reconfigurable nonlinear nonreciprocal transmission with an ultrahigh extinction ratio (over 30 dB) and low insertion loss (IL) for high transmission (less than 1.5 dB), as in the nonlinear regime (high input intensity) the transparency will only be present for one transmission direction. In the opposite direction, light will be channeled to another output, and we see a Lorentzian-shaped resonance, thus resulting in nonreciprocal transmission.

This approach also falls into the category of nonlinear nonreciprocal behavior, but it can be distinguished because of certain significant improvements. First of all, our circuit is implemented as an electrically tunable photonic circuit on a standardized, publicly available silicon photonics technology platform and could be potentially transplanted to any other integration platform that supports similar nonlinearities. While compared with other approaches in silicon PICs, like the use of cascaded asymmetric ring resonators with thermal nonlinearities [18,28] or an asymmetric silicon photonics crystal cavity [29], our device not only shows a much lower IL (1.5 dB) together with a high extinction ratio (over 30 dB), but also has a couple of significant features. First of all, the high/low transmission direction can be reconfigured by tuning the integrated heaters, which means that we can "program" the direction of high transmission. Prior results published in literature are limited to devices with no or limited tunability as they introduce the spatial asymmetry to different transmission directions at the design stage, making it a fixed feature of the circuit. While in our circuit, the physical structure is completely symmetric in the original state, but we can introduce and achieve dynamic reconfigurations of the spatial asymmetry by controlling the integrated heaters. Also, our approach does not require us to inject light in both transmission directions to have high intensity to trigger the nonreciprocal behavior [18,28,29]. Instead, it only requires the forward-propagating signal to have high power in order to trigger the low-loss transmission, while for the backward-propagating signal the transmission is always low irrespective of its power level. Because the device has four ports, it also has additional freedom: besides triggering the nonlinear behavior (transition from EIT resonance to a Lorentzian resonance) with high input intensity, a separate pump laser could be employed to remove the requirement on the input intensity.

Various all-optical functions could be built on this phenomenon. Even though this circuit might not be suitable for applications like an optical isolator, it could offer great value for applications like optical logic, computing, and signal processing, where silicon photonics are emerging as a promising platform. [30–35].

2. LINEAR CIRCUIT BEHAVIOR

The schematic of our circuit is drawn in Fig. 1. The main circuit is fabricated on a 200 mm silicon-on-insulator wafer using complementary metal-oxide-semiconductor (CMOS) technology in the IMEC standard passive silicon photonics platform [36]. Afterwards, two metal heaters are postprocessed in local Ghent University facilities to implement phase shifters. The waveguide layer is 220 nm thick, with a 2 μm thick buried oxide. The circuit consists of a ring resonator with two tunable reflectors inside. Each tunable reflector itself is a subcircuit consisting of an Mach–Zehnder interferometer (MZI) and a waveguide that connects its two outputs, forming a loop mirror [37,38]. By tuning the metal heater on top of one arm of the MZI reflector, its power reflectivity can be tuned efficiently, with only 0.5π needed to change the reflectivity from 0 to almost 100% [39]. The total round trip length of the ring resonator is about 1.1 mm, as each arm of the MZI reflector has a length around 200 μm (including bend sections) in order to ensure adequate phase shift using integrated heaters. But, it could be safely reduced to less than 20 μm with good quality heaters. The couplers of the ring resonator are designed to be identical for the critical coupling condition, each one has a designed coupling coefficient about 0.1, and the waveguide loss is measured around 1.8 dB/cm. The measured Q factor of a Lorentzian resonance from such a device is about

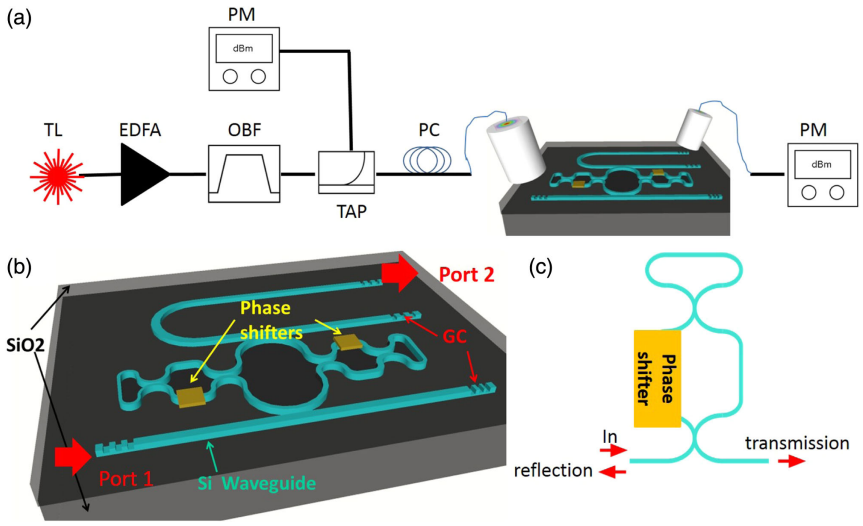

Fig. 1. (a) Setup to characterize the linear behavior of the device under test (DUT). TL, tunable laser; OBF, optical bandpass filter; Tap, a 1/99 splitter; PM, powermeter; PC, polarization controller. (b) The schematic of the DUT. GC, grating coupler. It is integrated on a silicon-on-insulator substrate. (c) The schematic of the tunable reflector in the DUT.

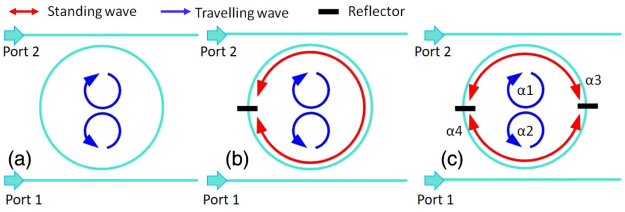

Fig. 2. Resonant modes in (a) a pure ring resonator, a ring resonator (b) with a single internal reflector and (c) with two internal reflectors. No matter whether light is injected into port 1 or port 2, (a) and (b) always have identical power distribution among their respective modes, while for (c), depending on the injection direction, the modes α_3 and α_4 could have very different intensity distribution. Thus, the structure generates a different transmission spectrum depending on transmission direction.

44,000, which facilitates a low threshold for the thermal nonlinearity. Increasing the coupling coefficient could lead to a smaller IL for the Lorentzian resonance transmission, but at the price of higher nonlinear threshold due to the increase of cavity loss.

The characterization of the device for low optical input power is performed using the setup shown in Fig. 1. An Agilent 8163B tunable laser with 1 pm wavelength step size is used as the source. The output will be first amplified by an erbium-doped fiber amplifier (EDFA) followed by a tunable optical filter to filter the noise of the EDFA. Then, a 1/99 tap is used to split the input light to a HP powermeter and the device under test (DUT). The powermeter helps to monitor the exact input power to the DUT. Grating couplers (GCs) are used to couple light from fiber to the chip and vice versa [40]. Each GC is expected to introduce around 6 dB IL near the measurement wavelength, based on separate measurements of reference circuits. The output of the DUT is connected to the Agilent photodetector to record the received power. Other equipment (not depicted) includes two Keithley 2400 source meters used to control the two metal heaters as well as a temperature controller underneath the photonics chip to stabilize the ambient temperature of the chip.

The linear behavior of the device has been reported in detail in Refs. [27,41,42]. Since we do not have access to directly monitor the performance of the individual reflector inside the cavity, we precharacterized and calibrated the phase shifters in the linear (low-power) regime by inspecting the spectra and matching them to circuit simulations of the circuit. When the power at the input of the DUT is as low as −5 dBm, low enough so that no nonlinearities are present, four different types of resonances at the drop port could be generated depending on the tuning conditions of the two metal heaters:

- A Lorentzian resonance [Fig. 3(a)] when both reflectors introduce zero reflections or the reflections caused by two reflectors have complete destructive interference. In this case, there would be only one corresponding traveling wave mode inside the cavity at a given input port as shown in Fig. 2(a). The peak transmission shows about 0.9 dB IL, indicating the ring is critically coupled.
- Autler–Townes splitting [43] [Fig. 3(a)], when only one reflector starts to show reflectivity. This reflection will couple the two circulating modes and lift their degeneracy [44]. Thus, they are resonant at slightly different frequencies but with identical intensity inside the resonator at steady state. Also, a standing wave would exist due to the internal reflector as plotted in Fig. 2(b). The splitting distance is proportional to the reflectivity, and it reaches the maximum at 0.5 × FSR when the reflectivity increases to 100% [45]. This could be interpreted in another way: under such circumstances, the two traveling waves would disappear with only the standing wave left. Since the standing wave cavity has double optical length compared with the ring resonator, the FSR of the standing wave is half of that of the traveling wave cavity.
- Fano resonance [Fig. 3(b)], when both reflectors introduce reflections. Now the two reflectors would form two Fabry–Perot (FP) cavities with standing modes as illustrated in Fig. 2(c). It has been demonstrated that the interaction of a discrete mode (high-Q) with a smooth background mode (low Q) would generate a Fano resonance when there is frequency detuning [41,46–48]. In our circuit, the two standing modes of the low-Q FP cavities serve as the background modes for the discrete modes corresponding to the ring resonances. But, the Fano resonance pattern has a qualitative difference compared with previously reported Fano resonances [49–52], since in our circuit the ring resonance is not a single Lorentzian resonance, but instead shows splitting, which can be modeled by two closely spaced Lorentzian resonances. Thus, it actually generates a double-Fano pattern.
- EIT [Fig. 3(c)]. Tightly linked to the appearance of the (double) Fano resonance, when the low-Q FP mode and the high-Q resonance have zero frequency detuning, a phenomenon called EIT will be triggered [23,27], with an ultranarrow bandwidth and usually large extinction ratio. This regime is the key for our device to exhibit large forward-to-backward extinction ratio and low IL at

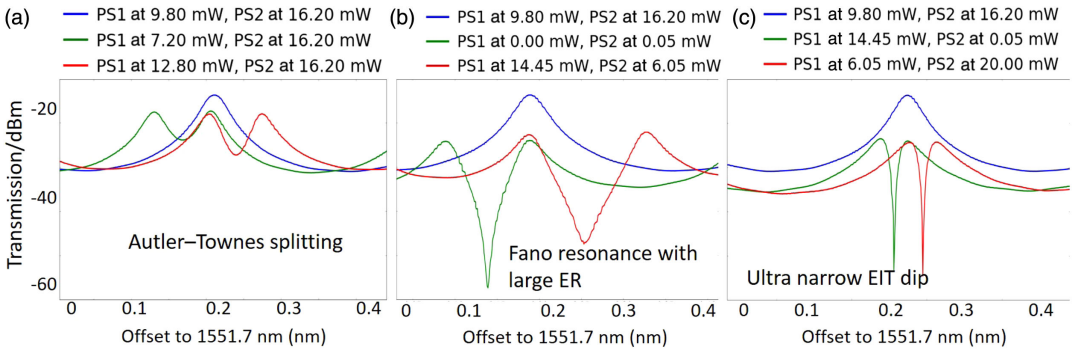

Fig. 3. When the input power is low such that no nonlinearities inside the cavity are triggered, there can be four kinds of resonances at its output, depending on the tuning conditions of the two phase shifters. (a) Lorentzian resonance with or without splitting. (b) Fano resonance with sharp slope. (c) Ultranarrow and deep EIT dip. Note that, in (a)–(c), the second peak can appear at either the left or right side of the original peak, depending on the tuning conditions.

the nonlinear nonreciprocal transmission. The frequency detuning between the FP modes and the ring resonances could be tuned by controlling the two reflectors. After all, the tiny amount of power is negligible to change the magnitude of the reflectivity (or Q-factor of the FP modes).

One important feature to highlight here: for the Autler–Townes splitting, Fano resonance, and EIT, the second peak can appear either blueshifted or redshifted with respect to the original peak depending on the operating conditions of the two phase shifters as evident in Figs. 3(a)–3(c), which is the key feature to realize reconfigurable nonreciprocal transmission.

3. NONLINEAR CIRCUIT BEHAVIOR

When the input power is increased to a certain value (over 0 dBm at the input of the DUT), thermal nonlinearities in the cavity will be induced around the resonance wavelength. The resonance spectrum will show distortion and will redshift compared with the undistorted resonance peak in the linear regime, as evident in Fig. 4, because the strong field inside the resonator will induce self-heating, which in turn changes the refractive index of the silicon waveguide [18,53,54,55]. At the Lorentzian resonance or Autler–Townes splitting regime, this distortion is independent of the transmission directions [Figs. 4(a) and 4(b)], which means the spectrum is identical irrespective of the transmission direction.

Interestingly, the distortion of the Fano resonance becomes dependent on the transmission direction at high input powers. The Fano resonance in the nonlinear regime is plotted in Figs. 4(c) 4(d) (the resonances are shifted vertically with spacing of 20 dB in order to provide a clear comparison). We define the transmission from port 1 to port 2 as T_{12} and vice versa. The left peak of the resonance is defined as P_1 and the right one as P_2. The feature is that either P_1 or P_2 shows the distortion is transmission dependent. In such a way, the behavior of the device becomes dependent on the transmission direction of the light, resulting in a nonreciprocal transmission with large forward-to-backward extinction ratio, as evident in Fig. 4(e). We are also able to determine which peak to distort by tuning the reflectors, as shown in Figs. 4(c) and 4(d), and therefore we can reconfigure the nonreciprocal transmission. In other words, we could determine which direction will exhibit high transmission, and the corresponding reverse direction will have low transmission. However, we do notice that at the nonlinear Fano resonance regime, the IL is relatively high (9 dB) as splitting is present for both transmission directions, which reduces the overall peak transmission [Fig. 4(e)]. In order to keep the nonreciprocal transmission with both large extinction ratio and low IL, we should use the EIT phenomenon as plotted in Fig. 5. Nonlinearities will still distort the EIT peak, dependent on the transmission direction. For the high transmission direction, the nonlinearities eliminate the EIT peak, leading to a distorted Lorentzian resonance with high transmission. This is because the device is configured such that the left peak P_1 experiences the nonlinearity, and therefore the two peaks come closer together until the resonance degenerates into a nonsplit Lorentzian resonance. This way, the IL is dramatically reduced to only 1.5 dB, as shown in Fig. 5. The IL is directly dependent on the configuration of the ring resonator, including its propagation loss and coupling coefficients. Increasing the coupling coefficients could potentially lead to a even smaller IL but at the price of higher nonlinear threshold. The working bandwidth that exhibits nonreciprocal transmission is 60 pm,

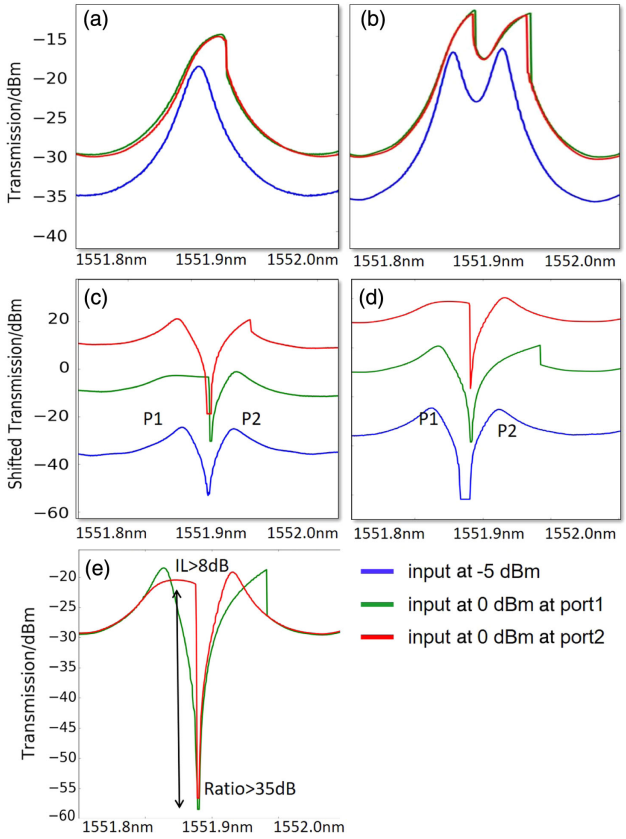

Fig. 4. When the input power is high, nonlinearity-induced distortion will emerge for all types of resonances. The green curve represents the transmission from port 1 to port 2 at high input power, while the red curve shows the reverse transmission at high input power. The blue curve refers to the transmission from port 1 to port 2 at low input power (without nonlinearities). (a) and (b) confirm that the spectra are identical at the Lorentzian resonance and the Autler–Townes splitting case, irrespective of the transmission direction. The high-power curves, obtained with a wavelength sweep from blue to red, show the characteristic roll-over indicative of thermo-optic nonlinear bistable behavior in the ring [53]. However, when the ring is configured into a Fano resonance, the distortions of the Fano resonances in (c) and (d) become dependent on the transmission direction; thus, nonreciprocal transmission is generated. Note that the red and green curves are offset in (c) and (d) for clarity. In (e), both curves are overlaid.

but it could be significantly increased by reducing the total ring length. For the opposite transmission direction, it is the right peak P_2 that shows nonlinearity and will experience a redshift, so the EIT peak is still present with much lower transmission, resulting a transmission suppression of over 30 dB. This highlights a key benefit of our device: for the backward-propagating wave, we do not require high power. The desired (low) transmission is the same in both the linear and nonlinear regime, because irrespective of the backscattered intensity, there is always an EIT dip with very low transmission. Similar to the Fano regime, we are able to dynamically configure the device to have high transmission in either one of the two possible directions, and low transmission in the other one.

The measurements discussed above were done by sweeping the input wavelength continuously from short to long wavelengths. Because for high input power the ring resonator will exhibit a bistable regime near the resonance [53,55], the wavelength sweep will only show one branch of this bistable regime and then abruptly

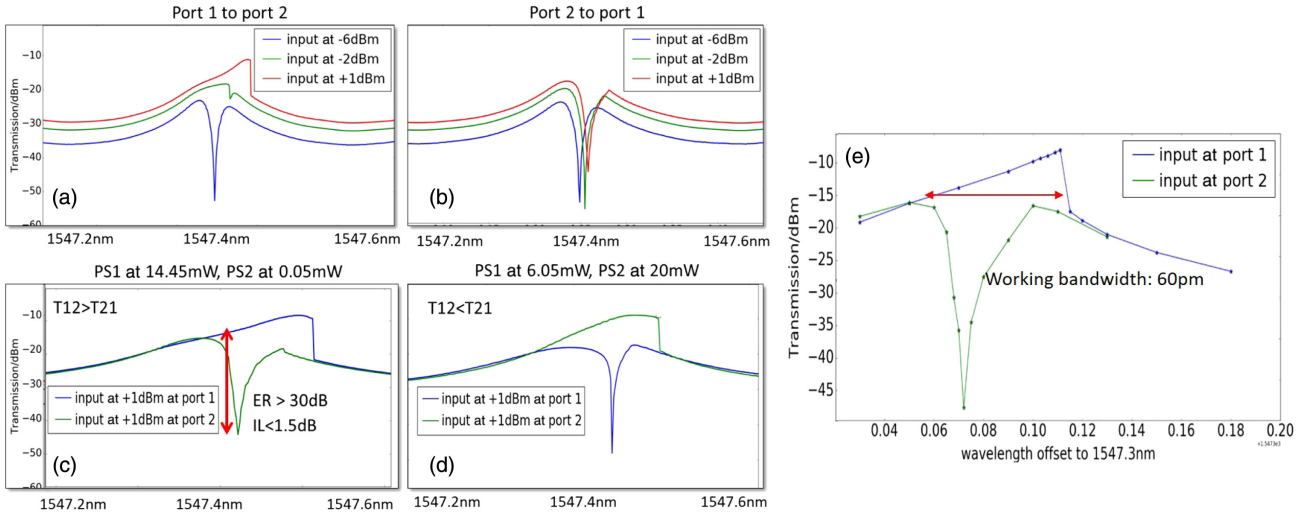

Fig. 5. Measurements of the nonlinear nonreciprocal transmission through the circuit configured for EIT. (a) Transmission spectra from port 1 to port 2 at varying input power. Note how the EIT peak evolves to a Lorentzian resonance and ends up with high transmission for high powers. (b) Spectra from port 2 to port 1 with varying input power; the EIT peak with low transmission is always present. This leads to nonreciprocal behavior with transmission from port 1 to port 2 as the high transmission direction as plotted in (c). (d) Device transmission in a configuration where transmission from port 2 to port 1 is higher than the opposite direction to confirm the reconfigurability of the high/low transmission direction. (e) Manual scan of discrete wavelength points to confirm the nonreciprocal transmission.

transition to the other branch. To show that the nonreciprocal transmission is not dependent on this particular sweep direction, we perform a manual scan with fixed input power at +1 dBm, where we turn off the laser for each step, then set the input wavelength and turn the laser back on to record the transmitted power, and then repeat this for each wavelength. The results are plotted in Fig. 5(e). The nonreciprocal pattern clearly persists.

The principle behind the nonlinear nonreciprocal transmission at the Fano/EIT regime is the asymmetric intensity localization within the ring cavity for the different transmission directions. To confirm this, we build a circuit model in Caphe to provide insights of the intensity distribution in the four quadrants of the ring resonator. The circuit model was drawn in Fig. 6(a). Each virtual tap is a dimensionless component that monitors the field passing through it without affecting field properties (both amplitudes and phase). We place four taps at the four quadrants of the ring resonator to monitor the individual intensity. When the ring operates at Lorentzian or Autler–Townes splitting conditions, the optical

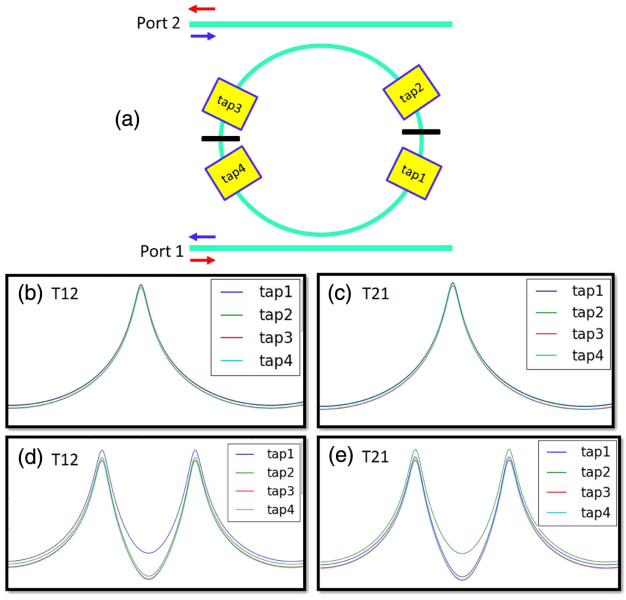

Fig. 6. (a) Circuit model to capture the intensity distribution at different sections of the ring resonator. Black solid lines represent reflectors. (b) and (c) Intensity profile at the Lorentzian resonance condition of transmission direction T_{12} (from port 1 to port 2) and T_{21}, respectively. (d) and (e) Results for when the ring operates at Autler–Townes splitting condition. Under both cases, the intensity profiles are identical for both transmission directions T_{12} and T_{21}; thus, the device is reciprocal.

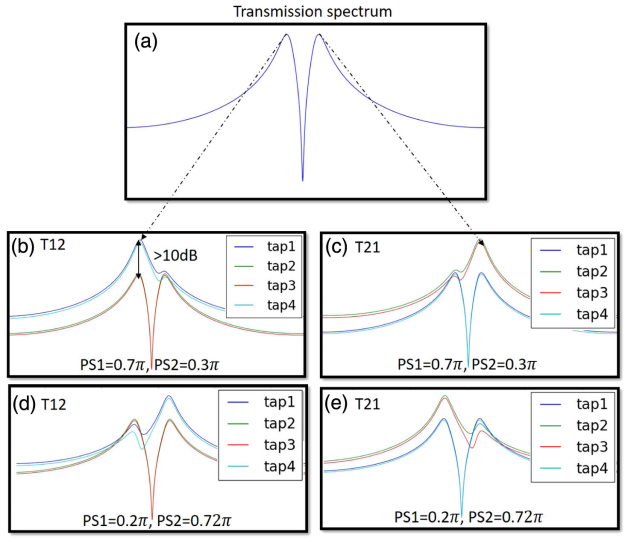

Fig. 7. (a) Linear power transmission spectrum under the EIT condition. (b) and (c) Intensity profile at four quadrants of the ring resonator at transmission directions T_{12} and T_{21}, respectively. Now different transmission directions lead to asymmetric intensity distribution. With high input power, it is the left peak of T_{12} that exhibits thermal nonlinearity-induced resonance redshift and would gradually eliminate the EIT dip, resulting in high transmission, while it is the right peak at T_{21} that shows resonance shift, and the EIT dip persists. (d) and (e) Results for different EIT conditions, under which the high/low transmission direction is switched.

intensities around resonances in the four quadrants are identical for both transmission directions T_{12} (from port 1 to port 2) and T_{21} (from port 2 to port 1) as evident in Figs. 6(b)–6(e); thus, the device is reciprocal no matter if it operates in the linear or nonlinear regime. While in the EIT condition, the intensity distribution shows a discrepancy between the two transmission directions, as plotted in Fig. 7. Specifically, when light goes from port 1 to port 2 (T_{12}), the intensity is mainly confined in the bottom part of the ring (tap1 and tap4), while for the reverse transmission direction (T_{21}), the intensity is confined in the top part (tap2 and tap3). The difference at the resonance wavelength can be larger than 10 dB. Thus, when the input power is high, the T_{12} transmission spectrum would exhibit a nonlinear shift that affects the left peak, which then gradually leads to the elimination of the EIT dip and results in a high transmission with a distorted Lorentzian shape. While for the opposite direction, it is the right peak that experiences a thermal-nonlinearity-induced resonance shift as now the optical intensity in the top section of the ring (tap2 and tap3) is much higher. So, the EIT pattern persists, and the transmission is low at the EIT wavelength. Consequently, nonreciprocal transmission is generated with T_{12} being the high transmission and T_{21} the low transmission. Figures 7(d) and 7(e) confirms the reconfigurability of the high/low transmission direction. When we change the working conditions of the two phase shifters, we still could get an EIT pattern, but now, at T_{12} transmission direction, the intensity is mostly confined at the top section of the ring (tap2 and tap3), and the right peak will exhibit nonlinear shift, while for T_{21}, it is now the left peak that exhibits nonlinear resonance shift. Under this circumstance, we make T_{12}/T_{21} the low/high transmission direction.

This device with nonlinear nonreciprocal transmission may not be suitable to function as a true optical isolator, but it would be of great interest to be used for nonlinear signal processing or a nonlinear switch that routes energy among its four ports based on the signal of the power. For instance, it could be used as a optical comparator or signal regenerator that detects a digitally modulated optical signal with reference to a threshold power. Power larger than this threshold is detected as "1" and lower as "0." The threshold could be set close to the trigger point of this nonlinear behavior (EIT → Lorentzian), and then the "1" signal will end up with very high transmission with negligible loss (1 dB) while the "0" signal will be considerably lost by the device. As a consequence, the extinction ratio of the digitally modulated signal will be dramatically boosted. Our device utilizes thermal nonlinearities, which act on a time scale of μs and thus are not suitable for high-speed data rates. However, the fundamental principle is self-phase modulation (optical intensity-dependent refractive index). So, the concept could be implemented in platforms with fast nonlinear effects like Kerr effect or free carrier dispersion in silicon [56].

4. PUMP–PROBE EXPERIMENT

Up until now, we have described a mode of operation that required the input power of the forward direction to be high enough in order to the induce thermal nonlinearity in the ring resonator to generate high transmission. However, the nonlinear transition from EIT to Lorentzian resonance can also be triggered using a separate pump

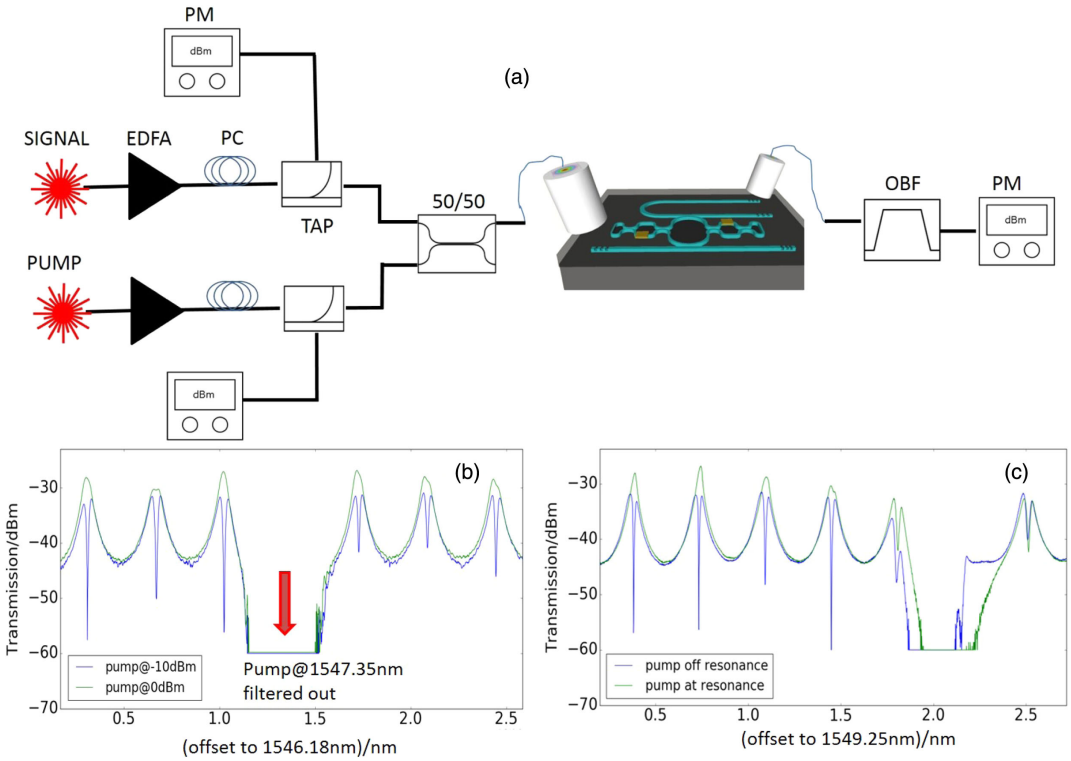

Fig. 8. Pump–signal measurement. (a) Measurement setup. A high-power pump laser and a low-power signal laser are mixed through a 50/50 coupler and fed into port 1 of the DUT together. The pump laser is fixed at a certain wavelength while the signal laser is swept at 1 pm step. (b) Spectra of the signal laser at different pump powers with the pump wavelength aligned to one of the resonance wavelengths. Clearly, when the pump power is high, the device generates a high transmission Lorentzian resonance. It behaves like a switch to the device to control the signal transmission. (c) Measured spectra at fixed pump power but with different pump wavelengths. Only when the pump is at the resonance wavelength, the transition from an EIT-like resonance to a Lorentzian resonance can happen.

laser to induce the asymmetric intensity distribution among the two standing wave modes.

To characterize it, we use a Santec TL510 tunable laser source (C-band) as the separate pump laser and perform some measurements in a pump–probe setup. For all the measurements, the device is configured to allow high transmission (for high power) from port 1 to port 2 and low transmission (for all powers) reversely. In the following section, with "power," we mean the power at the input of the DUT.

First of all, the pump laser is tuned to a resonance wavelength (1547.35 nm), and it is coupled with the signal laser through a 50/50 coupler before being fed into port 1. The setup is in Fig. 8(a). By setting the signal power to be very low (−10 dBm), we plot the spectra of the signal laser measured at port 2 with two pump levels as shown in Fig. 8(b). Clearly, at a low pump level (−10 dBm), the spectrum shows an EIT pattern, while when the pump levels increase to 0 dBm, the EIT pattern has disappeared and a single Lorentzian resonance is present as the pump is building up inside the cavity while making the desired changes to the cavity transmission. To further confirm the impact of the pump laser, we set the pump power at 0 dBm and measure the spectra at different pump wavelengths; one is at resonance (1551.09 nm), and the other one is off-resonance (1551.01 nm) as plotted in Fig. 8(c). When the pump laser is off-resonance, the EIT pattern is still observed as now the pump laser could not accumulate inside the cavity.

These two measurements confirm that by using a separate pump laser, even for a weak input signal, the EIT pattern could be converted to a Lorentzian resonance and lead to high transmission. Then, the device could support applications like all-optical switching, all-optical logic, and nonlinear signal processing. For instance, the device could be used as an all-optical "AND" logic gate with two inputs (pump and signal). If either of them is high (1), the output of the device would be high (1), while the output would be low (0) in case both of them have low power (0). Another example is that the device could be considered as a all-optical D-type flip-flop, with the pump laser serving as the control signal, and the transmission from input to output would only be allowed at high level of the control signal. Once again, even if our device is using thermal effects, the concept should also work with other fast nonlinear effects that make it more suitable for higher data rates.

5. CONCLUSION

In this paper, we propose a programmable photonics integrated circuit that is fully integrated onto silicon substrate with dynamic electrical tuning ability. It is a mixed cavity system supporting four modes inside the cavity. Using two metal heaters, the individual modes and the coupling between them can be efficiently controlled, as well as the corresponding output of the system. Various resonance patterns have been observed and explained, including Lorentzian resonance, split resonance, Fano resonance, and optical analogue of EIT. The behavior of the device at high input power (sufficient to induce thermal nonlinearity) is characterized in detail, and it is observed that at Lorentzian resonance or a split resonance pattern, the device is reciprocal, while at Fano resonance or EIT regimes, the device exhibits nonlinear nonreciprocal behavior, due to the asymmetric intensity distribution among the modes inside the cavity. Specifically, at one transmission direction, the nonlinearity-induced resonance distortion can eliminate the EIT transmission dip and result in a Lorentzian resonance with high transmission, while for the opposite direction, the EIT transmission dip remains, and therefore the circuit has a low transmission. This nonlinear nonreciprocal transmission is accompanied with an ultrahigh extinction ratio over 30 dB and low IL of about 1.5 dB, which exhibits significant improvement compared with previously demonstrated nonreciprocal transmission in silicon PIC. More importantly, we could configure the high/low transmission direction by tuning the metal heaters, making it a unique circuit for nonlinear nonreciprocal effects. Moreover, we experimentally demonstrate another all-optical approach to trigger the transition from an EIT pattern to a Lorentzian resonance, which is using a separate pump laser at one of the resonance wavelengths to generate the necessary mode conditions inside the cavity. This circuit could form the basis of a variety of optical functions, including but not limited to all-optical switching, all-optical flip-flop, all-optical signal regeneration, and all-optical logic gates.

REFERENCES

1. S. Fan, R. Baets, A. Petrov, Z. Yu, J. D. Joannopoulos, W. Freude, A. Melloni, M. Popović, M. Vanwolleghem, D. Jalas, M. Eich, M. Krause, H. Renner, E. Brinkmeyer, and C. R. Doerr, "Comment on 'nonreciprocal light propagation in a silicon photonic circuit'," Science **335**, 38 (2012).
2. D. Jalas, A. Petrov, M. Eich, W. Freude, S. Fan, Z. Yu, R. Baets, M. Popović, A. Melloni, J. D. Joannopoulos, M. Vanwolleghem, C. R. Doerr, and H. Renner, "What is—and what is not—an optical isolator," Nat. Photonics **7**, 579–582 (2013).
3. Z. Yu and S. Fan, "Complete optical isolation created by indirect interband photonic transitions," Nat. Photonics **3**, 91–94 (2009).
4. N. A. Estep, D. L. Sounas, J. Soric, and A. Alù, "Magnetic-free non-reciprocity and isolation based on parametrically modulated coupled-resonator loops," Nat. Phys. **10**, 923–927 (2014).
5. D. L. Sounas and A. Alù, "Non-reciprocal photonics based on time modulation," Nat. Photonics **11**, 774–783 (2017).
6. S. Fan, Y. Shi, and Q. Lin, "Nonreciprocal photonics without magneto-optics," IEEE Antennas Wireless Propag. Lett. **17**, 1948–1952 (2018).
7. M.-C. Tien, T. Mizumoto, P. Pintus, H. Kromer, and J. E. Bowers, "Silicon ring isolators with bonded nonreciprocal magneto-optic garnets," Opt. Express **19**, 11740–11745 (2011).
8. S. Ghosh, S. Keyvavinia, W. Van Roy, T. Mizumoto, G. Roelkens, and R. Baets, "Ce:YIG/silicon-on-insulator waveguide optical isolator realized by adhesive bonding," Opt. Express **20**, 1839–1848 (2012).
9. L. Bi, J. Hu, P. Jiang, D. H. Kim, G. F. Dionne, L. C. Kimerling, and C. Ross, "On-chip optical isolation in monolithically integrated non-reciprocal optical resonators," Nat. Photonics **5**, 758–762 (2011).
10. Y. Shoji and T. Mizumoto, "Magneto-optical non-reciprocal devices in silicon photonics," Sci. Tech. Adv. Mater. **15**, 014602 (2014).
11. D. Huang, P. Pintus, C. Zhang, P. Morton, Y. Shoji, T. Mizumoto, and J. E. Bowers, "Dynamically reconfigurable integrated optical circulators," Optica **4**, 23–30 (2017).
12. T. Mizumoto, R. Baets, and J. E. Bowers, "Optical nonreciprocal devices for silicon photonics using wafer-bonded magneto-optical garnet materials," MRS Bull. **43**(6), 419–424 (2018).
13. C.-H. Dong, Z. Shen, C.-L. Zou, Y.-L. Zhang, W. Fu, and G.-C. Guo, "Brillouin-scattering-induced transparency and non-reciprocal light storage," Nat. Commun. **6**, 6193 (2015).
14. J. Kim, M. C. Kuzyk, K. Han, H. Wang, and G. Bahl, "Non-reciprocal Brillouin scattering induced transparency," Nat. Phys. **11**, 275–280 (2015).
15. Z. Shen, Y.-L. Zhang, Y. Chen, C.-L. Zou, Y.-F. Xiao, X.-B. Zou, F.-W. Sun, G.-C. Guo, and C.-H. Dong, "Experimental realization of optomechanically induced non-reciprocity," Nat. Photonics **10**, 657–661 (2016).
16. L. D. Bino, J. M. Silver, M. T. Woodley, S. L. Stebbings, X. Zhao, and P. Del'Haye, "Microresonator isolators and circulators based on the intrinsic nonreciprocity of the Kerr effect," Optica **5**, 279–282 (2018).
17. F. Ruesink, J. P. Mathew, M.-A. Miri, A. Alù, and E. Verhagen, "Optical circulation in a multimode optomechanical resonator," Nat. Commun. **9**, 1798 (2018).

18. L. Fan, J. Wang, L. T. Varghese, H. Shen, B. Niu, Y. Xuan, A. M. Weiner, and M. Qi, "An all-silicon passive optical diode," Science **335**, 447–450 (2012).
19. A. M. Mahmoud, A. R. Davoyan, and N. Engheta, "All-passive nonreciprocal metastructure," Nat. Commun. **6**, 8359 (2015).
20. B. Peng, Ş. K. Özdemir, F. Lei, F. Monifi, M. Gianfreda, G. L. Long, S. Fan, F. Nori, C. M. Bender, and L. Yang, "Parity–time-symmetric whispering-gallery microcavities," Nat. Phys. **10**, 394–398 (2014).
21. X. Jiang, C. Yang, H. Wu, S. Hua, L. Chang, Y. Ding, Q. Hua, and M. Xiao, "On-chip optical nonreciprocity using an active microcavity," Sci. Rep. **6**, 38972 (2016).
22. S. Ramelow, A. Farsi, Z. Vernon, S. Clemmen, X. Ji, J. Sipe, M. Liscidini, M. Lipson, and A. L. Gaeta, "Strong nonlinear coupling in a Si_3N_4 ring resonator," Phys. Rev. Lett. **122**, 153906 (2019).
23. M. Fleischhauer, A. Imamoglu, and J. P. Marangos, "Electromagnetically induced transparency: optics in coherent media," Rev. Mod. Phys. **77**, 633–673 (2005).
24. K. Totsuka, N. Kobayashi, and M. Tomita, "Slow light in coupled-resonator-induced transparency," Phys. Rev. Lett. **98**, 213904 (2007).
25. Q. Xu, S. Sandhu, M. L. Povinelli, J. Shakya, S. Fan, and M. Lipson, "Experimental realization of an on-chip all-optical analogue to electromagnetically induced transparency," Phys. Rev. Lett. **96**, 123901 (2006).
26. X. Yang, M. Yu, D.-L. Kwong, and C. W. Wong, "All-optical analog to electromagnetically induced transparency in multiple coupled photonic crystal cavities," Phys. Rev. Lett. **102**, 173902 (2009).
27. A. Li and W. Bogaerts, "Tunable electromagnetically induced transparency in integrated silicon photonics circuit," Opt. Express **25**, 31688–31695 (2017).
28. M. Xu, J. Wu, T. Wang, X. Hu, X. Jiang, and Y. Su, "Push–pull optical nonreciprocal transmission in cascaded silicon microring resonators," IEEE Photon. J. **5**, 2200307 (2013).
29. Z. Wu, J. Chen, M. Ji, Q. Huang, J. Xia, Y. Wu, and Y. Wang, "Optical nonreciprocal transmission in an asymmetric silicon photonic crystal structure," Appl. Phys. Lett. **107**, 221102 (2015).
30. M. Fujii, A. Maitra, C. Poulton, J. Leuthold, and W. Freude, "Nonreciprocal transmission and Schmitt trigger operation in strongly modulated asymmetric WBGS," Opt. Express **14**, 12782–12793 (2006).
31. C. Koos, P. Vorreau, T. Vallaitis, P. Dumon, W. Bogaerts, R. Baets, B. Esembeson, I. Biaggio, T. Michinobu, F. Diederich, W. Freude, and J. Leuthold, "All-optical high-speed signal processing with silicon-organic hybrid slot waveguides," Nat. Photonics **3**, 216–219 (2009).
32. S. Phang, A. Vukovic, T. M. Benson, H. Susanto, and P. Sewell, "A versatile all-optical parity-time signal processing device using a Bragg grating induced using positive and negative Kerr-nonlinearity," Opt. Quantum Electron. **47**, 37–47 (2015).
33. N. R. Bernier, L. D. Toth, A. Koottandavida, M. A. Ioannou, D. Malz, A. Nunnenkamp, A. Feofanov, and T. Kippenberg, "Nonreciprocal reconfigurable microwave optomechanical circuit," Nat. Commun. **8**, 604 (2017).
34. Z. Li, M.-H. Kim, C. Wang, Z. Han, S. Shrestha, A. C. Overvig, M. Lu, A. Stein, A. M. Agarwal, M. Lončar, and N. Yu, "Controlling propagation and coupling of waveguide modes using phase-gradient metasurfaces," Nat. Nanotechnol. **12**, 675–683 (2017).
35. F. Lecocq, L. Ranzani, G. Peterson, K. Cicak, R. Simmonds, J. Teufel, and J. Aumentado, "Nonreciprocal microwave signal processing with a field-programmable Josephson amplifier," Phys. Rev. Appl. **7**, 024028 (2017).
36. P. Dumon, W. Bogaerts, R. Baets, J.-M. Fedeli, and L. Fulbert, "Towards foundry approach for silicon photonics: silicon photonics platform ePIX-fab," Electron. Lett. **45**, 581–582 (2009).
37. A. Li and W. Bogaerts, "Experimental demonstration of a single silicon ring resonator with an ultra-wide FSR and tuning range," Opt. Lett. **42**, 4986–4989 (2017).
38. A. Li and W. Bogaerts, "Backcoupling manipulation in silicon ring resonators," Photon. Res. **6**, 620–629 (2018).
39. A. Li, Q. Huang, and W. Bogaerts, "Design of a single all-silicon ring resonator with a 150 nm free spectral range and a 100 nm tuning range around 1550 nm," Photon. Res. **4**, 84–92 (2016).
40. D. Vermeulen, Y. De Koninck, Y. Li, E. Lambert, W. Bogaerts, R. Baets, and G. Roelkens, "Reflectionless grating couplers for silicon-on-insulator photonic integrated circuits," Opt. Express **20**, 22278–22283 (2012).
41. A. Li and W. Bogaerts, "An actively controlled silicon ring resonator with a fully tunable Fano resonance," APL Photon. **2**, 096101 (2017).
42. A. Li and W. Bogaerts, "Using backscattering and backcoupling in silicon ring resonators as a new degree of design freedom," Laser Photon. Rev. **13**, 1800244 (2019).
43. B. Peng, Ş. K. Özdemir, W. Chen, F. Nori, and L. Yang, "What is and what is not electromagnetically induced transparency in whispering-gallery microcavities," Nat. Commun. **5**, 5082 (2014).
44. A. Li, T. Van Vaerenbergh, P. De Heyn, P. Bienstman, and W. Bogaerts, "Backscattering in silicon microring resonators: a quantitative analysis," Laser Photon. Rev. **10**, 420–431 (2016).
45. A. Li and W. Bogaerts, "Fundamental suppression of backscattering in silicon microrings," Opt. Express **25**, 2092–2099 (2017).
46. U. Fano, "Effects of configuration interaction on intensities and phase shifts," Phys. Rev. **124**, 1866–1878 (1961).
47. S. Fan, "Sharp asymmetric line shapes in side-coupled waveguide-cavity systems," Appl. Phys. Lett. **80**, 908–910 (2002).
48. B. Luk'yanchuk, N. I. Zheludev, S. A. Maier, N. J. Halas, P. Nordlander, H. Giessen, and C. T. Chong, "The Fano resonance in plasmonic nanostructures and metamaterials," Nat. Mater. **9**, 707–715 (2010).
49. C. Qiu, P. Yu, T. Hu, F. Wang, X. Jiang, and J. Yang, "Asymmetric Fano resonance in eye-like microring system," Appl. Phys. Lett. **101**, 021110 (2012).
50. B.-B. Li, Y.-F. Xiao, C.-L. Zou, X.-F. Jiang, Y.-C. Liu, F.-W. Sun, Y. Li, and Q. Gong, "Experimental controlling of Fano resonance in indirectly coupled whispering-gallery microresonators," Appl. Phys. Lett. **100**, 021108 (2012).
51. W. Zhang, W. Li, and J. Yao, "Optically tunable Fano resonance in a grating-based Fabry–Perot cavity-coupled microring resonator on a silicon chip," Opt. Lett. **41**, 2474–2477 (2016).
52. G. Zhao, T. Zhao, H. Xiao, Z. Liu, G. Liu, J. Yang, Z. Ren, J. Bai, and Y. Tian, "Tunable Fano resonances based on microring resonator with feedback coupled waveguide," Opt. Express **24**, 20187–20195 (2016).
53. G. Priem, P. Dumon, W. Bogaerts, D. Van Thourhout, G. Morthier, and R. Baets, "Optical bistability and pulsating behaviour in silicon-on-insulator ring resonator structures," Opt. Express **13**, 9623–9628 (2005).
54. V. R. Almeida and M. Lipson, "Optical bistability on a silicon chip," Opt. Lett. **29**, 2387–2389 (2004).
55. Q. Xu and M. Lipson, "Carrier-induced optical bistability in silicon ring resonators," Opt. Lett. **31**, 341–343 (2006).
56. J. Wang, L. Fan, L. T. Varghese, H. Shen, Y. Xuan, B. Niu, and M. Qi, "A theoretical model for an optical diode built with nonlinear silicon microrings," J. Lightwave Technol. **31**, 313–321 (2013).